invited paper

Identifying of boron in FSW steel samples through SIMS technology

JaeNam Kim[1,3*], SangUp Lee[2], HyoegDae Kwun[2], KwangSoo Shin[2], ChangYong Kang[3]

[1]Graduate Institute of Ferrous Technology, POSTECH, Pohang, Korea
[2]Center for Analysis and Assessment, RIST, Pohang, Korea
[3]Department of Metallurgical Engineering, Pukyong National University, Busan, Korea

*jnkims@postech.ac.kr

Improvement of bainitic hardenability is outstanding feature of the boron addition into iron and steel. It is well established that a hardenability peak is accomplished when the concentration of boron is about several to several tens of weight ppm. In the previous study, resistive anode encoder (RAE) of the secondary ion mass spectroscopy (SIMS) was used to map the distribution of ppm of boron in iron and steel with the overall quantification using cluster-polyatomic secondary ion species for both impurity, I_i and matrix, I_m to reduce the matrix effect. The quantification of the boron was proposed by retrospective depth profile from the RAE boron map. In this study, the relative sensitivity factors (RSFs) and calibration curve of the standard reference materials were examined and calculated to identify the dissolved boron concentration which might be originated from poly crystal boron nitride (PCBN) tool in friction stir welding (FSW) for steel samples. Retrospective depth profile and linear regression of the calibration curve provides the boron quantification in FSW steel samples. Dark contrast areas on the FSW steel samples were indentified higher boron concentration than bright areas. It is accounted that the combination of $^{11}B^{16}O_2$ and $^{56}Fe^{16}O$ as for I_i / I_m is a useful method of SIMS quantification from boron image in iron and steel with minimal number of standard reference materials.

1. Introduction

One of the difficulties of quantitative elemental SIMS analysis is matrix effect. Matrix effect is general expression used to describe differences in sensitivity for a given element in samples of different composition. This small change of matrix effect can result significant change in ionization efficiency and sputtering yield. The use of RSF can compensate for matrix effect when SIMS data are processed because the RSF is a relative measure of the ionization probability of a given element in a given matrix using calibration standard reference material (SRM). The efforts to investigate the behavior of trace boron in steel using SIMS have been performed many years [1-2].

In 1986, S. Hashimoto et al. [3] performed quantification of trace boron in steel using boron implanted into pure iron (99.99%) at a dose of $1\times10^{13}\sim5\times10^{16}$ ions/cm² as standard reference materials. Calibration curve ($^{43}BO_2$ / Fe^{2+} or $^{43}BO_2$ / $^{16}O^-$ which are polyatomic for impurity and monatomic for matrix) of these series of references was used quantification of 10, 25, 40 wt.ppm of boron in steels which are exactly same composition of C, P, S and almost equal composition of Si, Mn, Cr, Mo, V, Al and N to avoid strong matrix effect. However, it is practically impossible to have all RSMs for every combination of the elements and matrices. This trace boron quantification from map is long time interest in steel industry with minute effort and minimal number of standard reference materials. In the previous study [4], we found that the use of cluster-polyatomic secondary ion species ($^{11}B^{16}O_2$ /$^{56}Fe^{16}O$) can reduce the matrix effect of

very different composition of iron and steel using four SRMs. The main purpose of adding trace boron is the improvement in hardenability [5-7]. It is generally accepted that a hardenability maximum is reached when the quantity of born is between 3 and 15 ppm.

2. Boron imaging

There are two different type of forming an ion image in magnetic sector SIMS. In microprobe mode configuration, the primary ion beam is focused to a fine spot and rastered across the sample. Figure 1, (A) shows boron distribution in very low carbon steel using oxygen primary ion. Alternatively, in microscope mode, Fig. 1 (B),
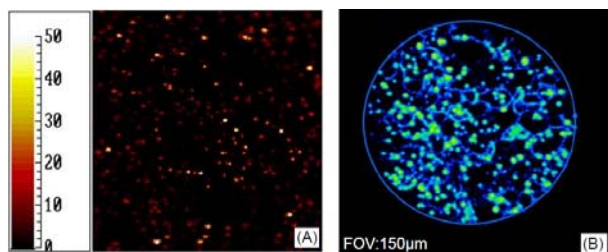
Fig. 1   Boron distribution of SIMS microprobe (A), and microscope mode (B) using RAE, respectively. Both samples are same low carbon steel, containing 5 ppm of born.

a broad area of the sample surface is illuminated by parallel, not focused and not rastered, primary ion beam. Resistive anode encoder (RAE) technique is based on the microscope mode. It is used to enhance the secondary ion intensity and convert the analogue information to digital information. It is position sensitive detector comprising a dual micro channel plate and resistive film coated on the ceramic plate. One of the advantages of RAE imaging mode is faster acquisition time than microprobe mode. Another attempt to boron study is neutron radiography so called particle tracking autoradiography (PTA) by neutron irradiation [2]. Figure 2 shows the variation of boron distribution of steels with different cooling speed and analytical mode, (A) obtained by RAE, (B) obtained by neutron radiography, respectively. RAE mode can be more clearly illustrated the grain boundary boron information than that of neutron radiography. Since the optics of the RAE mode use lens system it can easily magnify the secondary boron ion image. While, neutron radiography method is direct imprint α and Li particle on solid state nuclear detector film without lens optics system. Following equation is the resultant of neutron
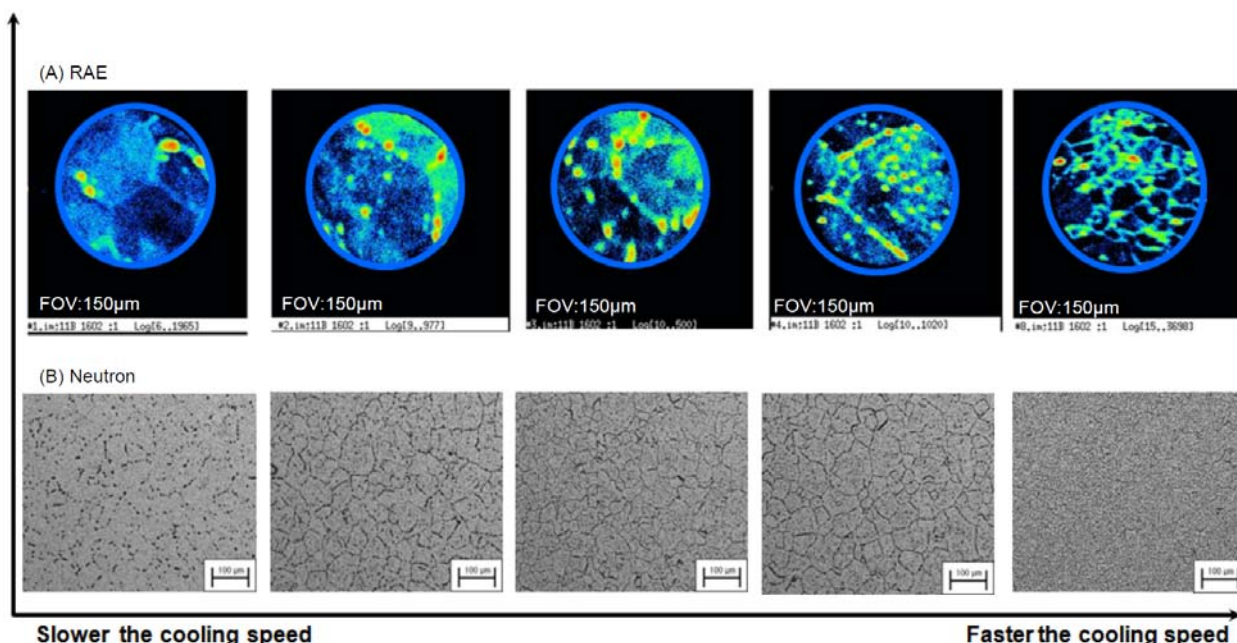
Fig. 2 Comparison of boron distribution images in steel as a function of cooling speed with different method, (A) SIMS microscope mode using RAE, and (B) Neutron radiography, respectively.

reaction with boron.

$$^{10}B + ^{1}n \rightarrow \, ^{4}\alpha + ^{7}Li + e \qquad (1)$$
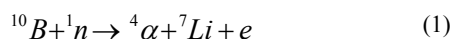
Another strong point of RAE map is faster acquisition time. RAE map greatly shortened the acquisition time of boron imaging from a day of neutron radiography to several minutes for one map. As shows in Fig 1, faster cooling rate lead the smaller grain size of the microstructure. Therefore, RAE boron imaging technique can be widely use for the metallurgical application field.

3. RSFs

The RSFs of the standard reference materials are measured and calculated from their relevant retrospective depth profiles of the RAE image. The chemical composition of the standard reference materials is listed Table 1.

Determination of RSF can be made by following equation.

$$RSF = \rho_i \frac{I_m}{I_i} \qquad (2)$$

where, ρ_i is the impurity atom density in atoms/cm^3, I_i is the secondary ion intensity of impurity in cps, and I_m is the secondary intensity of the matrix in cps. Table 2 summarized the RSF which were obtained from retrospective depth profile under different mass resolution for SRMs.

RSF$_B$ which is RSF of born was obtained using mass 43 of cluster-polyatomic ion and RSF$_C$ which is RSF of carbon was obtained using mass 12 of single-monatomic ion, respectively. The relative standard deviation (RSD) of the RSF$_B$ obtained at mass resolution of 2,000 was ±21.4%, whereas it was ±12% obtained at mass resolution of 4,500. It can be improve down to ±2.43% of RSD by discard SRM 1263A. Because, 0.24% of aluminum contained SRM1263A was greatly affected to the mass 43 which are coexist cluster-polyatomic $^{11}B^{16}O_2$ and $^{27}Al^{16}O$ at mass resolution of 2,000. More precisely, the former the mass is 42.99911 and the later the mass is 42.97645, respectively. ΔM of two species is 0.02266. It is considered that the use of 4,500 M/ΔM could eliminate the interference problem of this two ion species at mass 43, but need to compromise image field shadow-off in the RAE ion map [4].

As shown in Fig. 3, the RSF of carbon showed significant variation which was ±82% of RSD and this value is too big to accept as the useful RSF. It is demonstrated that the detection of single monatomic carbon is not entirely representative of the matrix composition. The detection of single monatomic $^{10}B^+$ or

Table 1   The chemical composition of the SRMs.
(Note: All units are wt. %, superscripts * indicate ppm.)

SRM	C	Si	Mn	Ni	Cr	Al	B	Fe
1263A	0.62	0.74	1.5	0.32	1.31	0.24	9*	Bal.
1264A	0.87	0.06	0.25	0.14	0.06	-	110*	Bal.
1265A	67*	80*	57*	0.04	70*	7*	1.3*	Bal.
C1151A	340*	0.29	2.37	7.25	22.59	30*	10*	Bal.

Table 2   Comparison of calculated RSF$_B$ and RSF$_C$ at different mass resolution for SRMs.

Standard Reference Materials	2,000 (M/ΔM)		4,500 (M/ΔM)
	Retrospective depth profile		Raster depth profile
	RSF$_B$ (atoms/cm^3)	RSF$_C$ (atoms/cm^3)	RSF$_B$ (atoms/cm^3)
1263A	7.88E18	2.37E19	1.12E19
1264A	3.55E19	2.14E22	2.29E19
1265A	2.48E19	1.56E20	2.13E19
C1151A	3.35E19	8.05E20	1.98E19
RSD	±21.4%	±82%	±12%

Fig. 3   Variation of RSFs as a function of cluster-polyatomic boron and single monatomic carbon with different mass resolution and different matrix.

$^{11}B^+$ was not available under the negative secondary condition which is used in this study. Regardless of the boron state, which may segregation in the grain boundary or precipitation of different chemical species or soluble boron, every combination of $^{11}B^{16}O_2$ /$^{56}Fe^{16}O$ was detected for the different iron and steels matrices as shown in Table 1. The goal was accurate determination of total boron concentration with corresponding boron ion map. The matrix effect arises not only by the boron state but also by the alloying elements and thermo mechanical treatment which will rather strongly contribute to the distinctive microstructure of iron and steels matrices.

4. Calibration Curve

The signal information of the direct ion image from the SIMS RAE can be computed by the profiler as intensity versus time. For a given species of the image, the intensity for each data point was computed according to the following relationships,

$$I(t_n) = \frac{\sum_{i,j} P_n(i,j)}{T} \qquad (3)$$

where $P_n(i,j)$ is the pixel intensity in counts of the contour for the nth image planes, T is the integration time for each image and t_n is the total time spent measuring from the beginning of the analysis to the end of acquisition of the n image planes. Example of RAE images obtained using cluster-polyatomic ion for both impurity boron and matrix iron ($^{11}B^{16}O_2$ / $^{56}Fe^{16}O$) are shown in Fig. 4.   As mentioned before, S. Hashimoto et al. were used $^{43}BO_2$ / Fe^{2+} or $^{43}BO_2$ / $^{16}O^-$ which is polyatomic for impurity and monatomic for matrix. Corresponding retrospective depth profile for born and iron used equation (3) is shown in Fig. 5, respectively.

Calibration curve of the SRMs for boron concentration versus the corresponding cluster- polyatomic ion intensity ratio of $^{11}B^{16}O_2$/$^{56}Fe^{16}O$ was made from retrospective depth profile or raster depth profile and shown in Fig. 6.
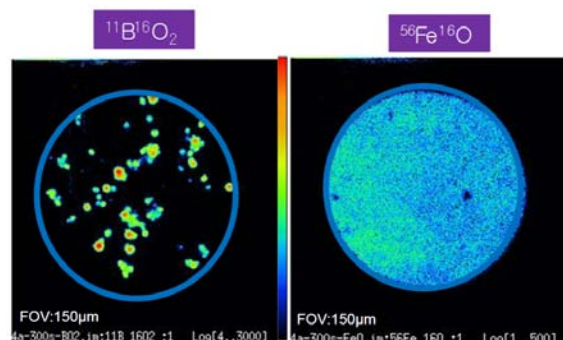
Fig. 4   RAE image of boron and iron cluster -polyatomic ion of SRM 1263A.
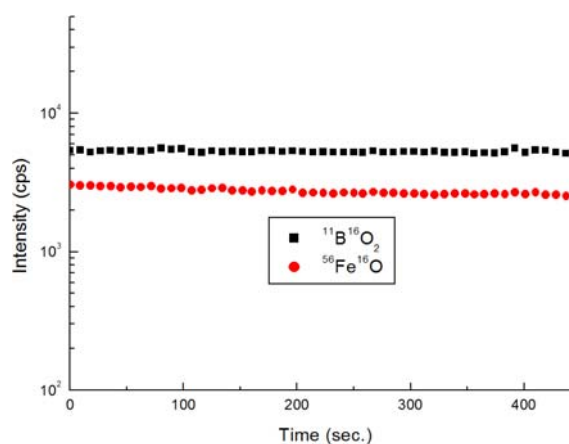
Fig. 5   Retrospective depth profile from RAE images of Fig. 4.

Two straight lines are drawn on each calibration curve in Fig. 6 by linear fitting using Origin software with the fit curve option of 95 confidences, 20 points, 15 range margins, and 1 fixed slope. The red solid lines fitted all four SRMs and black broken lines fitted three SRMs and discard the outlier of 1263A which contains 0.24 wt. % of aluminum. The correlation coefficient of the calibration curve is improved from 0.9349 to 0.9965 for the fitting of red solid line when it was carried out using 4,500 of mass resolution. These results is kept derivative of the mass interference of aluminum. However, aluminum concentration ranging from 7 to 30 ppm which corresponds to SRM of 1265A and C1151A (refer to Table 2) didn't affect on the cluster-polyatomic secondary ion intensity of $^{11}B^{16}O_2$. For this case, the correlation coefficient improved to 0.9999 at both M/ΔM of 2,000 and 4500.
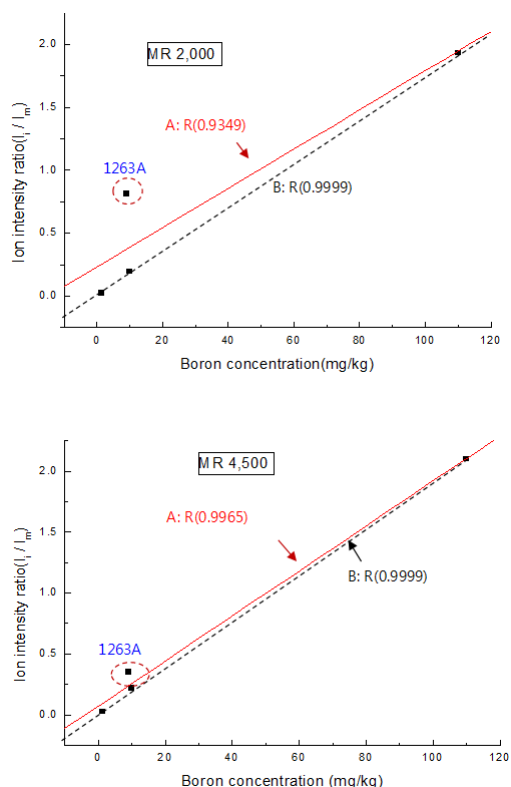
Fig. 6   Calibration curves between secondary ion intensity ratios versus boron concentration with two different mass

5. Identifying of boron in FSW steel samples

FSW is a solid state materials joining process which has been widely investigated in mostly low melting aluminum alloy. It was limited primarily to the application of joining of steels and other high temperature materials by the absence of suitable tool materials that can operate at high temperature [8]. Several distinguished research works has been reported on the FSW of steel application [9-13]. The microstructure and mechanical property of FSW joint depend on the FSW parameters as well as base material. A poly crystal boron nitride (PCBN) is the frequently used FSW tool in the field of steel application.

Two FSW steel samples were prepared SIMS analysis. Both FSW samples have different contrast site by site, bright area and dark area. Effort to understand this contrast variation in the microstructure after the FSW joint sample was required to identifying the boron

behaviors such as the distribution of the boron in the microstructure and the concentration of the boron site by site. The RAE direct ion images of the FSW steel samples in SIMS microscopy mode, Fig. 7 was obtained using CAMECA IMS 6F instrument. It is need to set the smallest contrast aperture for the best image resolution. One more important consideration is the astigmatism from aperture and slits should be avoided during all the measurements. A field of view of 150 um in diameter was used to display the distribution of impurity boron properly. Counting time of each mass was 1.67 seconds and waiting time was 0.56 seconds for $^{11}B^{16}O_2$, and 1.67 seconds for
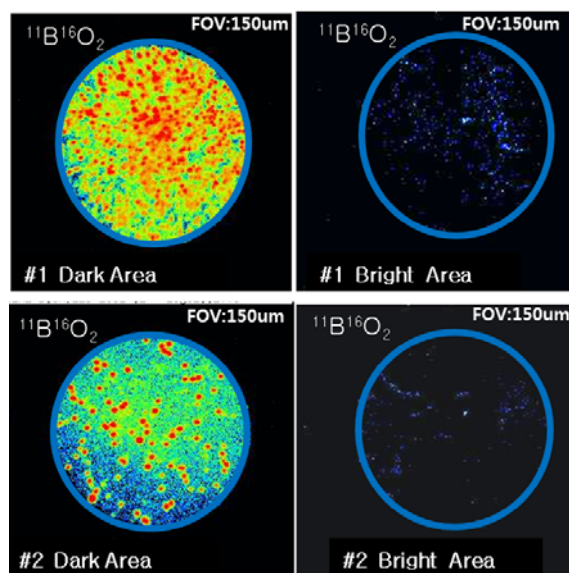
Fig. 7 RAE boron distribution images of the FSW steel samples.
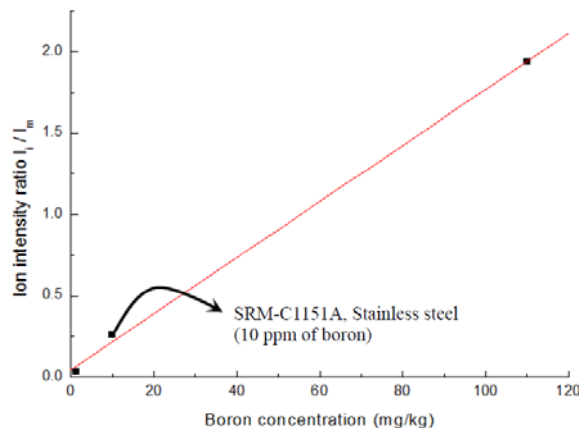
Fig. 8 Calibration curves of SRMs for FSW steel samples.

$^{56}Fe^{16}O$, respectively. A total of 50th image planes were stored for one map which was taken in about 3.3 minutes. Figure 7 shows dark area of the both FSW steel samples contains higher boron concentration than bright area. A calibration curve for FSW steel samples is shown in Fig. 8. Obtained boron concentration using calibration curve were 130.65 and 1.84 ppm for dark area and bright area in the sample #1. Meanwhile, the boron concentration of the dark area and bright area in the sample #2 were 48.79 and 0.91 ppm, respectively.

6. Conclusions

A combination of cluster-polyatomic ion of $^{11}B^{16}O_2$ and $^{56}Fe^{16}O$ as for I_i / I_m to quantify the boron in steel was made using FSW steel samples to confirm the feasibility of our earlier study which was the first trial to reduce the matrix effect and the suggestion of quantitative analysis of boron in iron and steel using calibration curve. It is considered that the combination of detection cluster-polyatomic secondary ion for both impurity and matrix species is useful method to reduce the matrix effect in SIMS quantification of boron in iron and steel. Dark contrast area on the micrograph of both FSW samples was identified higher concentration of boron than bright area. And the concentration of born difference was 60~80 times higher than bright area. The average reproducibility of the experiment was ±6.3% for RAE quantification according to the previous work.

7. Acknowledgments

8. References

[1] Ph. Maitrepierre, D. Thivellier, and R. Tricot, *Metall. Trans. A*, **6** , 287 (1975).

[2] M. Jahazi and J. J. Jonas, *Mat. Sci. Eng. A,* **335**, 49 (2002).

[3] S. Hashimoto, S. Doi, K. Takahashi, M. Terasaka, and M. Iwaki, *Mat. Sci. Eng.* **90**, 119 (1987).

[4] JaeNam Kim, SangUp Lee, HyeogDae Kwun, JoonWon Kim, KwangSoo Shin, and JungJu Lee, *Met. Mater. Int.* **18**, 361 (2012).

[5] I. S. Chung and S. G. Cho, *J. Kor. Inst. Met. Mater.* **31**, 1191 (1993).

[6] S. K. Banerji and J. E. Morral, *Conf. Proc.* pp. 1-215, TMS-AIME, Warrendale, PA, USA (1980).

[7] T. Zacharia, ICMCJP, pp. 153-160, American Welding Society, Orlando, Florida USA (1993).

[8] P. Threadgill, and R. Johnson, *Proc. 14th Int. Offshore and polar Eng. Conf.*, Toulon, France, ISOPE, pp. 1-7 (2004).

[9] T. J. Lienert, W. L.Stellwag, B. B. Grimmett, and R. W. Wake, *Welding Res., Supplt. to Welding J.* AWS, pp.1-5, (2003).

[10] R. Johnson, J. Dos Santos, and M. Magnasco, *4th Int. Friction Stir Welding Symp.,* Park City, Utah, USA, in CD-ROM, (2003).

[11] P. Konkol, *4th Int. Friction Stir Welding Symp.,* Park City, Utah, USA, in CD-ROM, (2003).

[12] K. Okamoto, S. Hirano, M. Inagaki, SHC. Park, YS. Sato, H. Kokawa, T. Nelson and Sorenson, *4th Int. Friction Stir Welding Symp.,* Park City, Utah, USA, in CD-ROM, (2003).

[13] M. Posada, J. DeLoach, AP. Reynolds, R. Fonda, and J. Halpin, *4th Int. Friction Stir Welding Symp.,* Park City, Utah, USA, in CD-ROM, (2003).